

NO-A106 831

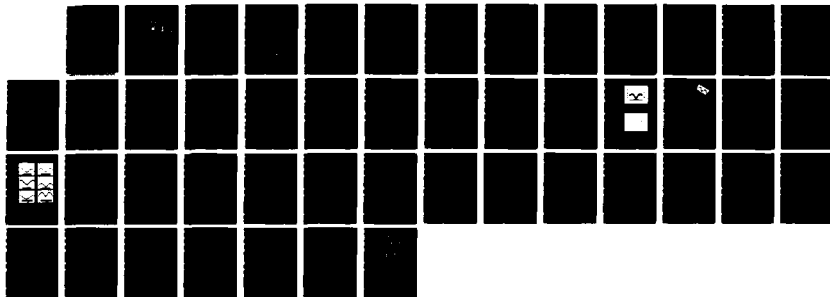
EMISSION ANGLES FOR SOFT X-RAY COHERENT TRANSITION  
RADIATION(U) NAVAL POSTGRADUATE SCHOOL MONTEREY CA  
R M ROBINSON SEP 87

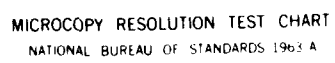
1/1

UNCLASSIFIED

F/G 20/8

NL





MICROCOPY RESOLUTION TEST CHART  
NATIONAL BUREAU OF STANDARDS 1963 A

AD-A186 851

2

# NAVAL POSTGRADUATE SCHOOL

Monterey, California

DTIC FILE COPY



DTIC  
ELECTE  
DEC 15 1987  
S D

## THESIS

EMISSION ANGLES FOR SOFT X-RAY  
COHERENT TRANSITION RADIATION

by

Robert Michael Robinson

September 1987

Thesis Advisor:

J.R. Neighbours

Approved for public release; distribution is unlimited

87 12 9 148

UNCLASSIFIED

SECURITY CLASSIFICATION OF THIS PAGE

## REPORT DOCUMENTATION PAGE

1a REPORT SECURITY CLASSIFICATION <b>UNCLASSIFIED</b>			1b RESTRICTIVE MARKINGS		
2a SECURITY CLASSIFICATION AUTHORITY			3 DISTRIBUTION/AVAILABILITY OF REPORT Approved for public release; distribution is unlimited		
2b DECLASSIFICATION/DOWNGRADING SCHEDULE					
4 PERFORMING ORGANIZATION REPORT NUMBER(S)			5 MONITORING ORGANIZATION REPORT NUMBER(S)		
6a NAME OF PERFORMING ORGANIZATION Naval Postgraduate School		6b OFFICE SYMBOL (if applicable) Code 61		7a NAME OF MONITORING ORGANIZATION Naval Postgraduate School	
6c ADDRESS (City, State, and ZIP Code) Monterey, California 93943-5000		7b ADDRESS (City, State, and ZIP Code) Monterey, California 93943-5000			
8a NAME OF FUNDING SPONSORING ORGANIZATION		8b OFFICE SYMBOL (if applicable)		9 PROCUREMENT INSTRUMENT IDENTIFICATION NUMBER	
8c ADDRESS (City, State, and ZIP Code)		10 SOURCE OF FUNDING NUMBERS			
		PROGRAM ELEMENT NO		PROJECT NO	TASK NO
					WORK UNIT ACCESSION NO
11 TITLE (Include Security Classification) <b>EMISSION ANGLES FOR SOFT X-RAY COHERENT TRANSITION RADIATION</b>					
12 PERSONAL AUTHOR(S) Robinson, Robert M.					
13a TYPE OF REPORT Master's Thesis		13b TIME COVERED FROM TO		14 DATE OF REPORT (Year, Month, Day) 1987, September	
				15 PAGE COUNT 46	
16 SUPPLEMENTARY NOTATION					
COSATI CODES			18 SUBJECT TERMS (Continue on reverse if necessary and identify by block number)		
FIELD	GROUP	SUB GROUP	Particle Beam Energy; Transition Radiation; Coherent/Incoherent; Emission Angle ←		
17 ABSTRACT (Continue on reverse if necessary and identify by block number)					
<p>Emission angles for both coherent and incoherent transition radiation in the soft x-ray region were measured. The results clearly show that coherent transition radiation produces larger emission angles at high beam energies than does incoherent radiation. These results allow the possibility of using coherent transition radiation to measure higher electron beam energies than are possible using incoherent radiation approximations. The measured emission angle magnitudes are compared to theoretical values obtained using computer simulation. Differences are noted and possible sources of error are cited.</p> <p style="text-align: right;"><i>(Signature)</i></p>					
19 DISTRIBUTION AVAILABILITY OF ABSTRACT <input checked="" type="checkbox"/> UNCLASSIFIED/UNLIMITED <input type="checkbox"/> SAME AS RPT <input type="checkbox"/> OTIC USERS			21 ABSTRACT SECURITY CLASSIFICATION Unclassified		
22a NAME OF RESPONSIBLE INDIVIDUAL Prof. John R. Neighbours			22b TELEPHONE (Include Area Code) (408) 646-2922		22c OFFICE SYMBOL Code 61Nb

Approved for public release; distribution is unlimited

Emission Angles for Soft X-Ray  
Coherent Transition Radiation

by

Robert Michael Robinson  
Lieutenant, United States Navy  
B.S., United States Naval Academy, 1980

Submitted in partial fulfillment of the  
requirements for the degree of

MASTER OF SCIENCE IN PHYSICS


from the


NAVAL POSTGRADUATE SCHOOL  
September 1987

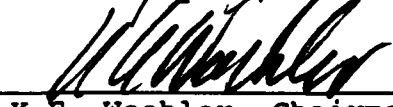
Author:

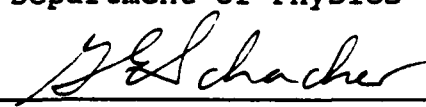
  
Robert Michael Robinson

Approved by:

  
John R. Neighbours, Thesis Advisor

  
Xavier K. Maruyama, Second Reader

  
K.E. Woehler, Chairman  
Department of Physics

  
G.E. Schacher,  
Dean of Science and Engineering

# ABSTRACT

Emission angles for both coherent and incoherent transition radiation in the soft x-ray region were measured. The results clearly show that coherent transition radiation produces larger emission angles at high beam energies than does incoherent radiation. These results allow the possibility of using coherent transition radiation to measure higher electron beam energies than are possible using incoherent radiation approximations. The measured emission angle magnitudes are compared to theoretical values obtained using computer simulation. Differences are noted and possible sources of error are cited.



Accession For	
NTIS CRA&I	<input checked="" type="checkbox"/>
DTIC TAB	<input type="checkbox"/>
Unannounced	<input type="checkbox"/>
Justification	
By	
Distribution	
Availability Codes	
Dist	Avail
A-1	

## TABLE OF CONTENTS

I.	INTRODUCTION -----	7
	A. BACKGROUND -----	7
	B. PURPOSE -----	8
	C. PREVIOUS EXPERIMENTS AT NPS -----	8
II.	THEORY -----	10
	A. THEORETICAL DEVELOPMENT -----	10
	B. COMPUTER SIMULATION -----	15
III.	THE EXPERIMENT -----	18
	A. EXPERIMENTAL SETUP -----	18
	B. PROCEDURE -----	20
IV.	RESULTS -----	25
	A. EXPERIMENTAL RESULTS -----	25
	1. Correction Factor from the Timing Method -----	27
	2. Comparison with Incoherent Radiation Method -----	28
	B. ADDITIONAL SOURCES OF ERROR -----	30
V.	CONCLUSIONS -----	32
	A. CONCLUSIONS -----	32
	B. RECOMMENDATIONS FOR FUTURE EXPERIMENTS -----	32
	APPENDIX A: NPS LINEAR ACCELERATOR -----	34
	APPENDIX B: HAMAMATSU LINEAR IMAGE SENSOR -----	36
	APPENDIX C: TARGET STACK CONSTRUCTION -----	39
	APPENDIX D: COMPUTER SIMULATION -----	41

LIST OF REFERENCES -----	43
INITIAL DISTRIBUTION LIST -----	45



### ACKNOWLEDGEMENTS

I express my thanks to my thesis advisor, Professor J.R. Neighbours, and especially to my second reader, Professor Xavier Maruyama, for their assistance in completing this thesis. I also want to thank Dr. M.A. Piestrup for his suggestions and assistance and Mr. D. Snyder for the operation of the LINAC. Finally, a very special thank you to my wife, Nancy, and my sons for their patience and cooperation.

## I. INTRODUCTION

### A. BACKGROUND

The existence of transition radiation was first predicted by V.L. Ginsburg and I.M. Frank in 1945 while the two were studying Cerenkov radiation [Ref. 1:pp. 353-362]. They noted the existence of radiation when conditions for Cerenkov radiation, including having electron velocity greater than the speed of light, were not met. The radiation occurring when a charged particle transits two media of differing dielectric constants is thus called transition radiation. Experimental observation of transition radiation was delayed because the radiation yield produced by a single dielectric pair interface is very small.

G.M. Garibyan caused a revival of interest in transition radiation in 1958 when he predicted that the energy of a moving particle was proportional to the total transition radiation yield. M.L. Cherry et al. demonstrated the coherent addition of radiation from multiple foil stacks and the use of transition radiation as a particle beam detector [Ref. 2:p. 3594].

Use of transition radiation to measure the energy of electrons in early studies was restricted by the absorption of the x-rays by multiple dielectric foil stacks. The high

degree of absorption restricted the radiation measured to the hard x-ray region [Ref. 2:p. 3594]. More recently, thin foil stacks allow measurements in the soft x-ray region (1 keV to 3 keV) [Refs. 3:p. 1771; 4:p. 1223].

#### B. PURPOSE

The energy of a beam of charged particles passing through a foil stack is proportional to the energy and inversely proportional to the spread of the emitted photons. Past experiments have shown that the incident particle beam energy can be found from the emission angle of incoherent transition radiation using the approximation  $\theta = 1/\gamma$ . This, however, limits the maximum value of measurable beam energy because of the precision required to measure small emission angles. The purpose of this report is to show that at high beam energies coherent transition radiation can produce significantly larger angles of emission than incoherent radiation. Coherent radiation could thus be used to measure higher incident beam energies.

#### C. PREVIOUS EXPERIMENTS AT NPS

Two recent experiments involving transition radiation have been conducted at NPS. Both efforts were completed in December 1986. Yoon Seog Koo measured the differential production efficiencies from foil stack materials for a 65 MeV electron-beam. This involved the prediction and measurement of emission cones and the manufacture of foil

stacks similar to those used in this experiment [Ref. 5:p. 3]. Yim Chang-Ho used measurements of the emitted x-ray cones to predict the energy of an incident electron beam. His work concentrated on radiation emitted from incoherent foil stacks [Ref. 6:p. 3]. Information gained from each of these experiments was used in the development of measurement techniques for this experiment.

## II. THEORY

### A. THEORETICAL DEVELOPMENT

Transition radiation is electromagnetic radiation which is emitted when a moving particle travels from one medium to another medium with a different dielectric constant. Unlike Cerenkov radiation, transition radiation does not require the particle to be traveling at a speed greater than the speed of light in the medium. Transition radiation is emitted in the form of concentric cones whose angle of emission is dependent on the energy of the moving particle (see Figure 2.1).

Transition radiation requires a sudden change in the dielectric constant and can occur only over a limited distance. The minimum distance over which it can occur is called the formation length, and is given by [Ref. 2:pp. 3695-3596]:

$$Z_i = \frac{23 c}{(1 - (\epsilon_i - \sin^2 \theta)^{1/2})} \quad (1)$$

where for x-rays  $\epsilon_i$  ( $i = 1, 2$ ) =  $1 - (\omega_i/\omega)^2$  are the permittivities of the two media,  $\omega_i$  are the media plasma frequencies,  $\beta = v/c$ ,  $v$  is the particle speed,  $c$  is the speed of light, and  $\theta$  is the emission angle. For near-relativistic electrons,  $\beta \sim 1$ . In addition, the emission

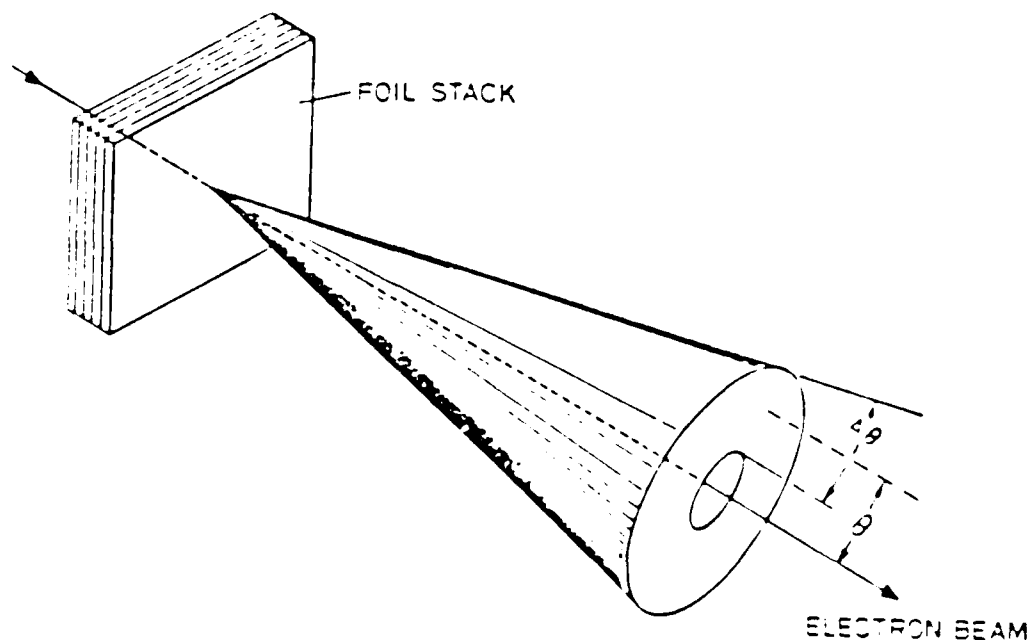


Figure 2.1 Transition Radiation is Emitted as Concentric Cones. The Magnitude of Emission Angle Depends on the Initial Energy of the Electron Beam.

angle is very small, so one can approximate  $\sin \theta \sim \theta$ . Using  $\gamma = (1-\beta^2)^{-1/2}$  and considering only the first term of the binomial expansion such that  $1/\gamma^2 = 2(1-\beta)$ , equation (1) becomes

$$z_i \sim \frac{4\lambda\beta}{(1/\gamma)^2 + \theta^2 + (\omega_i/\omega)^2} \quad (2)$$

where  $\lambda = (\text{wavelength})/2\pi$ . [Ref. 3:p. 1772]

The differential cross section for transition radiation production per frequency per unit solid angle is given by:

$$\frac{d^2 N(\omega)}{d\Omega d\omega} = F_1 * F_2 * F_3, \quad (3)$$

where  $N(\omega)$  is the transition radiation photon number and  $\omega$  is the angular frequency [Refs. 4:p. 1224; 7:p. 485].

The first factor,  $F_1$ , is the intensity of radiation produced per unit frequency and per unit solid angle from one electron crossing a single interface and is given by [Ref. 2:p. 3595]:

$$F_1 = \frac{\alpha\omega\sin^2\theta}{16\pi^2 c^2} (z_1 - z_2)^2, \quad (4)$$

where  $\alpha = (1/137)$  is the fine structure constant. Again, one can approximate  $\sin \theta \sim \theta$ , so the equation becomes:

$$F_1 = \frac{\alpha\omega\theta^2}{16\pi^2 c^2} (z_1 - z_2)^2. \quad (5)$$

The second factor,  $F_2$ , accounts for the coherent superposition of radiation from the two surfaces of the foil. If one ignores the incoherent effects of electron collisions within the foil and also the photon attenuation through the foil, this factor is approximately

$$F_2 = 4 \sin^2(l_2/Z_2) \quad (6)$$

where  $l_2$  is the thickness of the foil [Refs. 5:p. 486; 6:p. 487]. This term is maximized when  $(l_2/Z_2) = (m - 1/2)\pi$ , where  $m$  is an integer.

The third multiplying factor,  $F_3$ , is necessary to account for the combined contributions of several foils in a stack and the attenuation of x-rays traversing the stack. For "M" foils, this factor is given by:

$$F_3 = \frac{1 + \exp(-M\sigma) - 2\exp(-M\sigma/2)\cos(2MX)}{1 + \exp(-\sigma) - 2\exp(\sigma/2)\cos(2X)} \quad (7)$$

where  $\sigma = (u_1 l_1 + u_2 l_2)$  and  $u_{1,2}$  is the absorption coefficient of the mediums 1 and 2, and  $X = (l_1/Z_1 + l_2/Z_2)$  [Ref. 5:p. 483]. For vacuum spacing between foils,  $u_1 = 0$ . For high photon energies, x-ray absorption is negligible so that  $\sigma \sim 0$ . Then one can approximate

$$F_3 \sim \frac{1 + 1 - 2\cos(2MX)}{1 + 1 - 2\cos(2X)} = \frac{\sin^2(MX)}{\sin^2 X} \quad (8)$$



In order to obtain coherent addition of radiation from all surfaces,  $X = r\pi$ , where  $r$  is an integer. By taking the limit as  $X \rightarrow r\pi$  and using L'Hopital's Rule, the maximum value of  $F(M, X)$  is found to be:

$$\lim_{X \rightarrow r\pi} \frac{\sin(MX)}{\sin(X)} = \lim_{X \rightarrow r\pi} \frac{M \cos(MX)}{\cos(X)} = M.$$

Combining all three terms, the maximum value of radiation intensity in equation (3) is therefore

$$\frac{d^2 N}{d\Omega d\omega} = \frac{\alpha \omega \theta^2}{16\pi^2 c^2} (z_1 - z_2)^2 4M^2. \quad (9)$$

Replacing the expressions for  $z_i$  (equation (2)) in the resonance condition  $X = r\pi$ , the resonance condition for transition radiation may be written as:

$$\cos(\theta_r) = \frac{l_1 + l_2}{l_1 \sqrt{\epsilon_1} + l_2 \sqrt{\epsilon_2}} (1/\beta - r\lambda / (l_1 + l_2)), \quad (10)$$

where  $\theta_r$  is the emission angle at resonance [Refs. 8:p. 266; 9:p. 269]. For small emission angles, this equation can be approximated as:

$$\theta_r^2 = \frac{2r\lambda}{l} - \frac{1}{\gamma^2} - (\omega_0/\omega)^2, \quad (11)$$

where  $\omega_0^2 = (\omega_1^2 l_1 + \omega_2^2 l_2) / (l_1 + l_2)$  and  $l = l_1 + l_2$  [Ref. 8:p. 272]. Note that the angle of emission can be

significantly greater than  $(1/\gamma)$  at high energies and  $\omega \gg \omega_0$ . For incoherent transition radiation, the angle of emission is proportional to  $(1/\gamma)$ . Thus at high energies, incoherent radiation becomes unable to distinguish beam energies.

#### B. COMPUTER SIMULATION

Equation (10) provides a method for calculating the angle of emission from coherent transition radiation. This equation, however, provides the angle as a function of the material mode number, "r", and the photon wavelength, " $\lambda$ ". To predict the overall emission angles, a computer program was generated to sum the  $\theta_r$  values over many mode numbers. The program, generated by Adelphi Technologies, Inc., calculates the value of each term in the equation for many modal values [Ref. 8]. The resultant summation plotted photon flux versus emission angle. The peaks in photon flux occur at the locations of the emission cone. The computer program allowed varying each parameter of the equation, aiding the analysis of experimental results.

Figure 2.2 shows the output for a series of electron beam energies. An especially noteworthy result of the simulation is the increasing angle of emission as electron beam energy increases. The emission angle for incoherent radiation decreases as beam energy increases. This result, although not completely understood, was confirmed by the experiment. This particular graph was made using the same

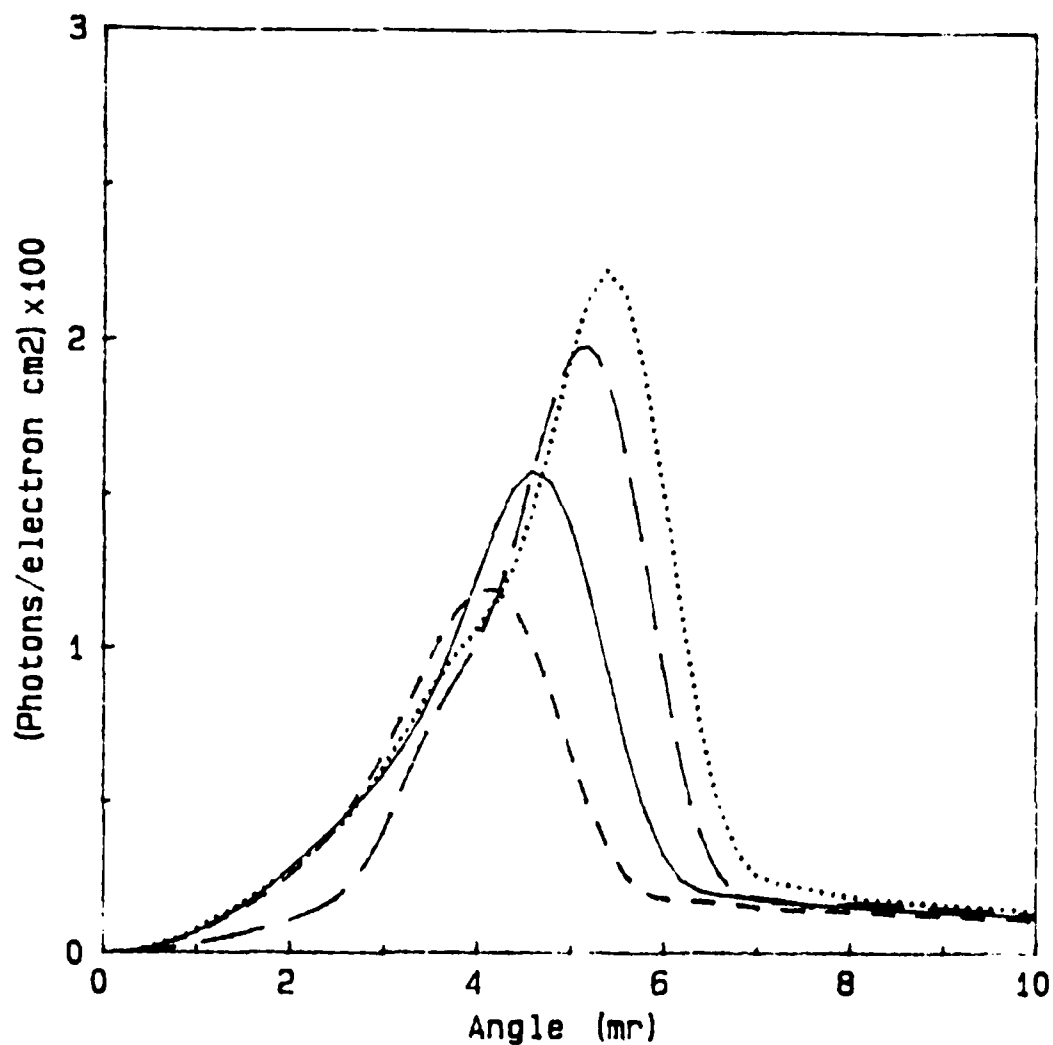


Figure 2.2 Emission Angles for Coherent Radiation at Various Electron Beam Energies. For a Set of Fixed Target Parameters, the Emission Angle Reaches a Maximum at High Energies. Varying the Parameters of the Target Stack Could Provide a Larger Spread in Angle Magnitudes at These Energies.

target parameters as the actual experiment: 8 foils, 3.5  $\mu\text{m}$  foil thickness, 8.5  $\mu\text{m}$  interfoil separation. A plasma frequency corresponding to energy of 24.1 eV was assumed throughout the program for mylar foils. Additional information on the choice of parameters in the program and the method of calculation is contained in Appendix D.

The program analyzes a range of photon energies from 0.1 keV to 4.0 keV, the range of the soft x-ray spectrum. (This range provides the values of  $\lambda$  in equation (10).) The program performs a summation over the range of integer values of  $r$  which yields a real value for  $\theta_r$  when used in equation (10). The electron energies chosen correspond to the electron beam energy levels most reliably obtained in the experiment. This graph was used to calculate the predicted emission angle values shown in Chapter IV.

### III. THE EXPERIMENT

#### A. EXPERIMENTAL SETUP

The experiment was performed using the electron linear accelerator (LINAC) at the Naval Postgraduate School (NPS). Detailed information on the LINAC can be found in Appendix A.

A. A diagram of the experimental apparatus used for production and detection of x-rays is shown in Figure 3.1.

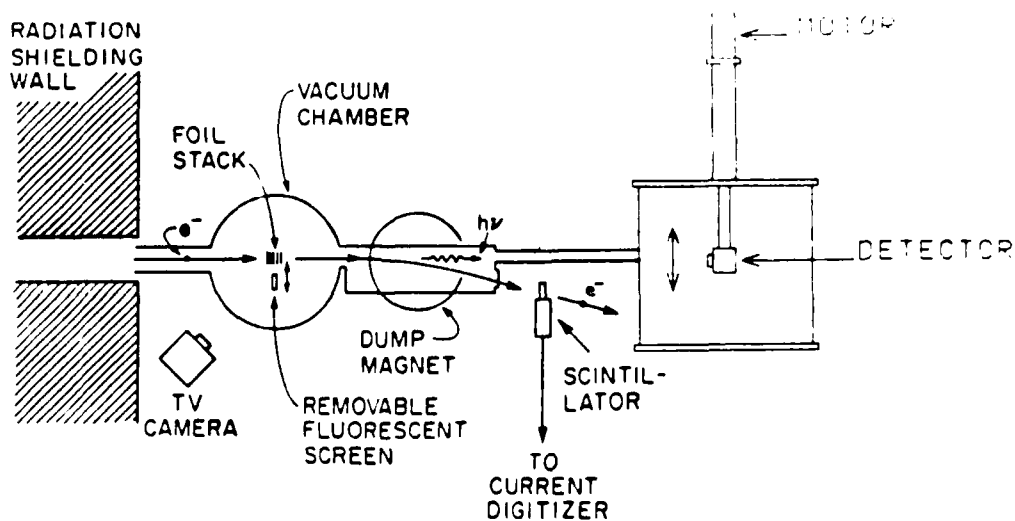


Figure 3.1 Diagram of the NPS LINAC Experimental Apparatus

Electrons exit the LINAC and strike the mylar foil stack in the vacuum chamber. The dump magnet allows the photons created to pass unhindered, but deflects the incident electron beam. The electron beam must be deflected from the detector since its high energy could cause permanent catastrophic damage to the detector, as well as bias results. The electron beam then passes through a scintillation detector and into a beam dump.

The photons which passed through the dump magnet entered a detection chamber which contained a HAMAMATSU Linear Image Sensor. This sensor is a linear array of 512 photodiodes placed side by side in a continuous line. Additional information on the sensor can be found in Appendix B. Detector output was directed to both an oscilloscope and a properly interfaced computer monitor. The size of the HAMAMATSU sensor allowed detection and measurement of the primary cones on either side of the initial beam axis. Measuring the physical separation of the output peaks corresponded to measuring the emission angle of the radiation. The detector could be raised into a shielded housing, protecting it from extraneous radiation when not actually required for the experiment.

The vacuum chamber contained a fluorescent screen and three target foil stacks connected on a movable column. The foil stacks included an eight foil coherent stack, an eight foil incoherent stack, and a single foil with mylar

thickness equivalent to that of the other stacks. Details on construction of the coherent target stack are contained in Appendix C. A remotely controllable worm screw motor allowed positioning either the screen or the desired target in the beam path. The target stacks could also be rotated to allow varying the angle of incidence of the electron beam. The fluorescent screen could be positioned in the beam path to allow aligning and focussing the electron beam.

#### B. PROCEDURE

Each run of the experiment began with the detector in the stowed (protected) position and the fluorescent screen in the electron beam path. The beam could then be focussed and aligned without damaging the detector. When the electron beam was correctly positioned, the dump magnet was turned on to deflect the electrons from the sensitive detector. Then the detector was lowered to the expected geometric center of the transition radiation cone. The incoherent stack was then lowered into the beam path and the output of detected radiation observed on the oscilloscope. The electron beam was then repositioned as necessary to center the transition radiation cone on the detector device. Due to the small magnitude of lateral adjustments with respect to the distance from the target to the detector, repositioning the beam was assumed to cause no change in the incident angle. The output of a properly positioned beam was characterized by easily discernible radiation output

peaks and a clearly defined valley, which corresponded to the axis of the electron beam (see Figures 3.1 and 3.2). When the beam was properly positioned, it was "tuned" by the LINAC operator to maximize clarity of the peaks and stabilize the output. (The frequent switching on and off of large electrical loads near the LINAC and the accompanying power surges made it difficult to maintain a steady electron beam.) When all adjustments were completed, photographs of the oscilloscope display were made (see Figure 3.3). The coherent beam was then rapidly placed in the electron beam path and its output photographed without repositioning the beam. When a satisfactory set of photographs was obtained, the energy of the electron beam was shifted and the process was repeated. Because of fluctuations in beam intensity, it was often necessary to make several runs at a single energy before acceptable results were obtained.

Additional sets of experiments were run with the target stacks rotated at various angles. These rotations changed the effective foil thicknesses and spacings to:

$$l_{1,2}^* = l_{1,2} / \cos \theta$$

where  $l_{1,2}$  is the actual foil thickness and spacing, and  $\theta$  is the angle between the electron beam and the normal to the foil surface.



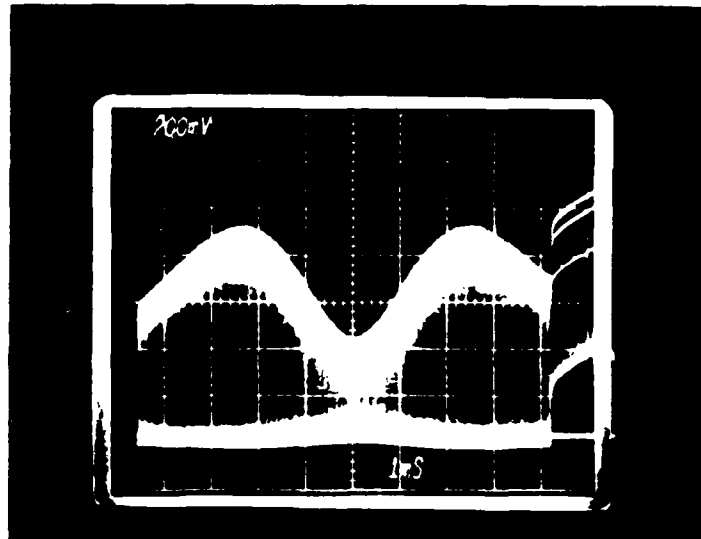


Figure 3.1 The Beam Axis (at the Valley) and the Peaks from Both Sides of the Emission Cone are Clearly Displayed on this Radiation Pattern from a 96 MeV Electron Beam Through the Incoherent Stack.

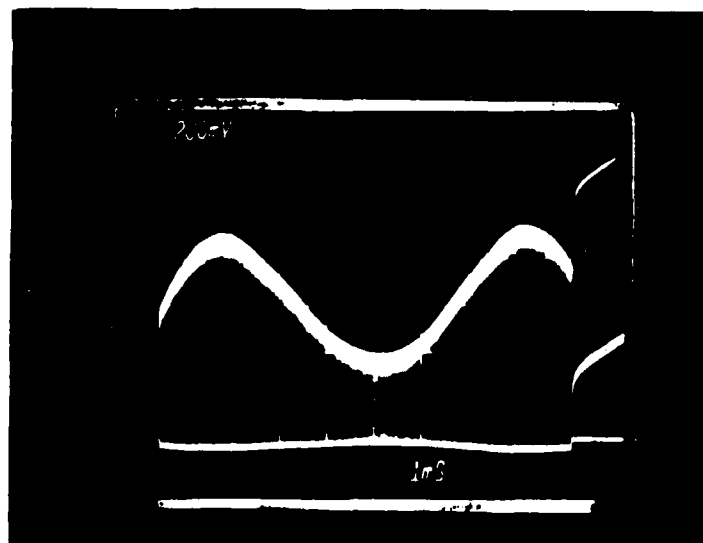


Figure 3.2 A Larger Emission Angle Prevents both Peaks from Being Shown on this Radiation Pattern from a 94 MeV Trace Through the Coherent Stack. The Beam was Shifted to Display the Valley and One Peak.

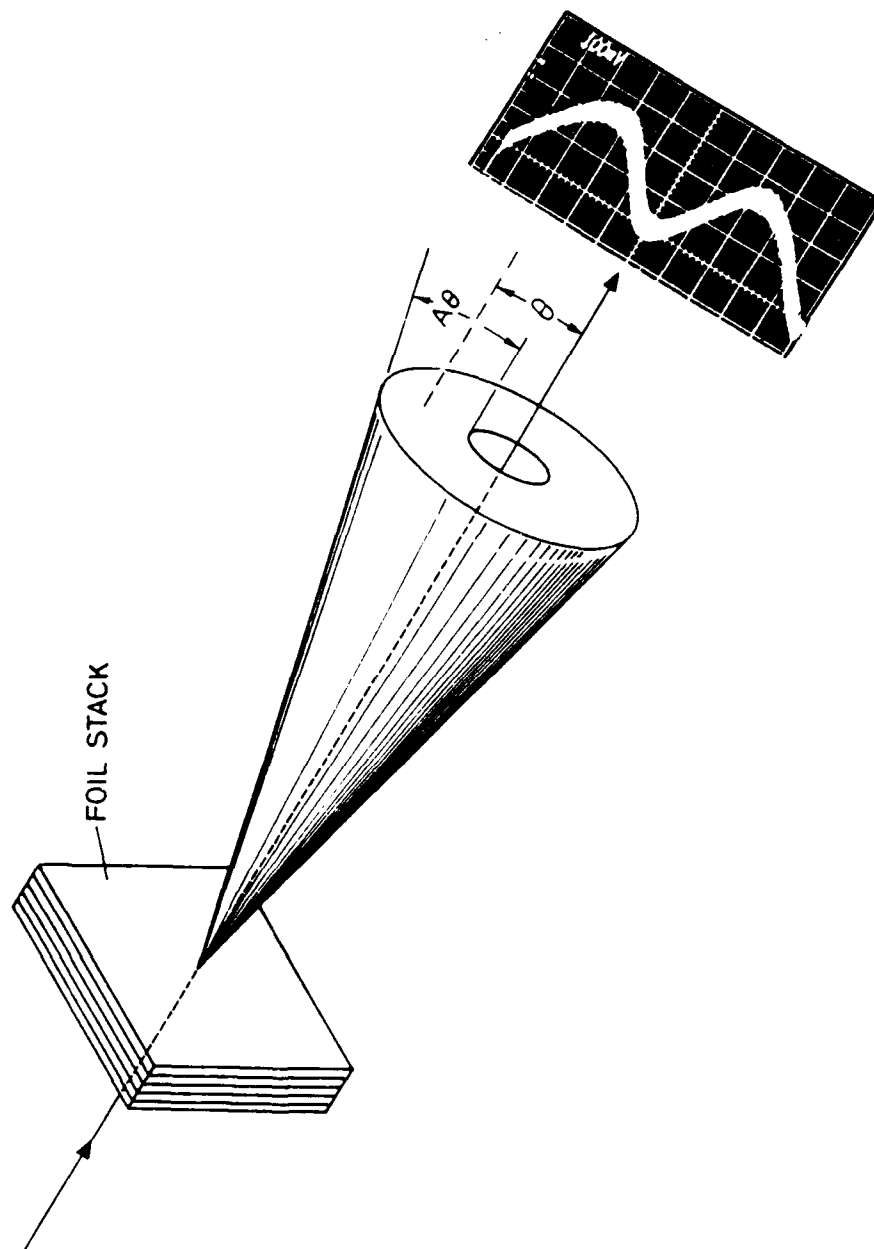


Figure 3.3 The Relationship between the Emission Cone and Oscilloscope Display is Shown. Notice the Well Positioned Beam.

The magnitude of emission angles could be calculated by measuring the peak to peak separation for each energy level. This spread was compared to the total spread of the output on the oscilloscope, which was assumed to correspond to the full width of the photodiode array. Since this width was known and the distance from the target stack to the detector was also known, simple geometry could be applied to find the emission angles. For example, using a detector width of 2.5 cm and a target stack to detector distance of 150 cm, a peak to peak spread of 6 units on a total display spread of 9 units yields an emission angle of

$$\theta_r = (1/2)(6/9)(2.5 \text{ cm}/150 \text{ cm}) = 5.5 \text{ mrad} .$$

(Note that the total peak to peak spread gives twice the emission angle, hence a factor of 1/2 must be applied.)

#### IV. RESULTS

##### A. EXPERIMENTAL RESULTS

Figure 4.1 provides a comparison of coherent and incoherent transition radiation emission patterns. The figures are photographs of the oscilloscope display and show the intensity of radiation received by the photodiode array versus the location on the array. These comparisons clearly show the different angle of emission for coherent transition radiation which was predicted by equation (11).

Measurements of the emission angle for coherent transition radiation yielded the values shown in Table 4.1 below. The calculated values differ widely from the values predicted by the theory (Figure 2.2). An investigation to find the reason for the disparity revealed an error in the electrical connection of the photodiode array which caused

TABLE 4.1  
COMPARISON OF MEASURED COHERENT AND INCOHERENT  
EMISSION ANGLES (UNCORRECTED)

<u>Beam Energy (MeV)</u>	<u>Incoherent <math>\theta</math> (mrad)</u>	<u>Coherent <math>\theta_c</math> (mrad)</u>
96.6	$4.44 \pm 0.6$	$5.47 \pm 0.4$
94.0	$4.01 \pm 0.4$	$6.90 \pm 0.4$
84.0	$4.90 \pm 0.4$	$7.13 \pm 0.4$
78.6	$4.50 \pm 0.4$	$5.97 \pm 0.4$

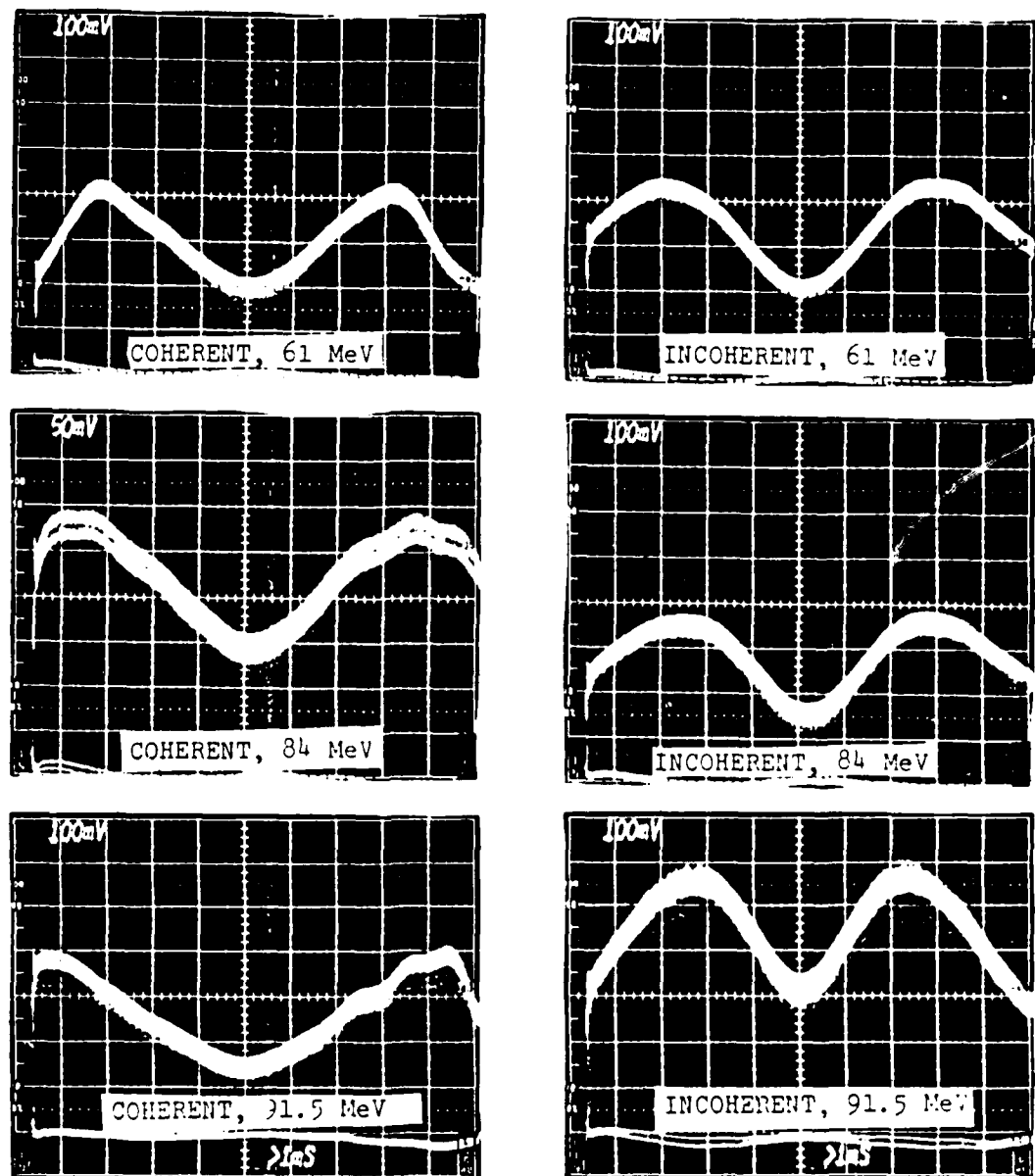


Figure 4.1 A Comparison of Emission Angles for Coherent and Incoherent Radiation. Note that the Larger Peak to Peak Spread for Coherent Radiation. Also Notice that the Spread Increases with Increasing Beam Energy for Coherent Radiation, but Decreases for Incoherent Radiation. (Horizontal Scales are Equal for All Six Cases.)

the array to read only a section of the diodes in the array. The error was not found until the procedural phase of the experiment was completed and the LINAC was reconfigured for a different project. Because of the error, full width on the oscilloscope trace did not correspond to the full width of the array. To make the results obtained from the experiment useful, a correction factor was required. This correction factor could not be well defined. Two approximations of the correction factor are described below.

1. Correction Factor from the Timing Method

The photodiode array is clocked at a rate of 200 kHz. Four complete clock cycles are required to read each individual diode, or a total of 2048 clock cycles to read the complete array. This corresponds to a period of 10.24 msec for the array. Photographs of the array output on the oscilloscope display indicated a period of just 8.8 msec. Assuming all diode cells are equal in size, this yields an effective array width of 2.2 cm. By adjusting the data to take into account this effective array width, corrected emission angle values were calculated.

The results obtained using this correction factor are shown in Table 4.2. Also shown are the predicted emission angle taken from Figure 2.2 and the variance between the two sets of values. This correction factor was found to be incomplete by comparing theoretical emission

TABLE 4.2  
CORRECTED EMISSION ANGLES USING THE TIMING METHOD

Electron Beam Energy (MeV)	Corrected Measured Incoherent Emission Angle (mrad)	Corrected Measured $\theta_r$ (mrad)	Theoretical Coherent $\theta_r$ (mrad) *	% Diff. in $\theta_r$
96.6	$3.70 \pm 0.6$	$5.62 \pm 0.4$	5.44	3.3
94.0	$4.18 \pm 0.4$	$7.78 \pm 0.4$	5.30	46.8
84.0	$4.41 \pm 0.4$	$6.36 \pm 0.4$	4.59	38.6
78.6	$4.59 \pm 0.4$	$6.73 \pm 0.4$	4.19	60.6

\*Theoretical coherent emission angle values obtained from computer simulation.

angles for incoherent radiation (found from  $\theta = 1/\gamma$ ) with the angles obtained from the adjusted data.

## 2. Comparison with Incoherent Radiation Method

The correction factor in this method was obtained after analyzing several runs of incoherent transition radiation. Assuming that the  $\theta_r = (1/\gamma)$  approximations held for this experiment and using the same relationships between emission angle and peak-to-peak separation on the oscilloscope display as described in Section III.B above, the effective photodiode array width could be calculated. For example, on Figure 4.1 for an energy of 84 MeV, the  $(1/\gamma)$  approximation predicts an emission angle of 6.08 mrad. For a target stack to detector distance of 135.1 cm, a peak

to peak distance of 1.64 cm is calculated. In the experiment, the peak to peak spread was actually 5.3 units, so that one unit on the oscilloscope display corresponds to 0.31 cm. Since the total output covers 9.6 units, the effective array width is 2.98 cm. Similar calculations were made at various energy levels and averaged. This produced an overall effective array width of 3.29 cm. Using this value of array width, coherent radiation emission angles were calculated as described in Section III. Results are shown in Table 4.3.

TABLE 4.3  
CORRECTED EMISSION ANGLES USING THE COMPARISON METHOD

Electron Beam Energy (MeV)	Theoretical Incoherent Emission Angle (mrad)	Corrected Measured $\theta_r$ (mrad)	Theoretical Coherent $\theta_r$ (mrad)	% Diff. in $\theta_r$
96.6	5.32	$8.33 \pm 0.4$	5.44	53.1
94.0	5.44	$9.98 \pm 0.4$	5.30	88.3
84.0	6.08	$9.25 \pm 0.4$	4.59	101.0
78.6	6.56	$8.98 \pm 0.4$	4.19	114.0

Inaccuracies in this method result from the large variance in peak-to-peak distances found at individual energies. These differences are believed to be due primarily to rapid fluctuations in electron beam intensity.



A comparison of theoretical emission angles and corrected measured values for both incoherent transition radiation and coherent transition is shown in Table 4.4.

TABLE 4.4  
THEORETICAL EMISSION ANGLES VERSUS CORRECTED ANGLES  
FOR INCOHERENT AND COHERENT TRANSITION RADIATION

Electron Beam Energy (MeV)	Incoherent Radiation Emission Angle (mrad)		Coherent Radiation Emission Angle (mrad)		
	Theory (1/γ)	Experimental Corrected	Theory (Fig. 2.2)	Experimental Correction Method	
				1	2
96.6	5.32	4.46	5.44	5.62	8.33
94.0	5.44	4.52	5.30	7.78	9.98
84.0	6.08	4.41	4.59	6.36	9.25
78.6	6.56	5.08	4.19	6.73	8.98

#### B. ADDITIONAL SOURCES OF ERROR

In addition to the incorrect connection of the photodiode array, the following possible sources of errors were noted:

1. The glue used in the construction of the foil stack was assumed to be planar and of infinitesimal thickness. Given the small magnitude of other stack parameters, the assumption of infinitesimal thickness may not be valid. Since any variation in glue film thickness decreases foil stack coherence, this assumption must be modified. The effect of this error source could be reduced by increasing the thickness of the foil layers and the interfoil separation distance, making variations in glue film thickness insignificant. Construction of stacks without the use of glue would eliminate the problem.

2. Large electrical equipment cycling on and off in the immediate vicinity of the LINAC caused significant, unpredictable fluctuations in the intensity of the electron beam. The gauge used to read beam intensity provides a time averaged value. Therefore it does not accurately indicate beam intensity during fluctuations. The instability of the beam was reflected on the oscilloscope display of emission patterns in the form of inconsistent peak heights and emission angles for outputs at supposedly equal beam energies.
3. The LINAC electron gun went out of commission shortly after completion of this experiment. If the electron pulse magnitudes were not stable due to the failing gun during the experiment, the emission patterns outputted would again be affected without any indication on the electron beam intensity gauge.

## V. CONCLUSIONS

### A. CONCLUSIONS

Coherent and incoherent transition radiation has been measured. Direct comparisons of the emission patterns for coherent transition radiation and incoherent transition radiation clearly show a larger emission angle for coherent radiation (Table 4.4). The increased magnitudes of coherent radiation emission angles allow the possibility of using coherent transition radiation for particle beam measurements at higher energies than possible with incoherent radiation and the  $\theta = 1/\gamma$  approximation.

The emission angle magnitudes obtained from the experiment do not match the theoretically predicted values for both coherent and incoherent radiation. The lack of agreement is not fully understood. Possible reasons for the differences are cited in Section IV.A and Section IV.B above. Correcting the sources of error should allow accurate estimates of initial electron beam energy from an analysis of the coherent transition radiation emission patterns.

### B. RECOMMENDATIONS FOR FUTURE EXPERIMENTS

A new foil stack with larger inter-foil spacing should be constructed. The increased distance between foils would minimize the effect of varying glue thickness and other

small irregularities. This would also increase the effect of rotating the target stack, providing an indication of emission angle size changes as coherence is approached.

The output of the electron beam energy detector should be directly referenced to the radiation emission output. In this way, the emission pattern could be normalized to a constant value, negating the effect of beam energy fluctuations.

A source of direct cooling to the photodiode detector should be provided to reduce the increase in dark current due to thermal effects. Without direct cooling, the increase in detector temperature contributes to a very large increase in dark current. Although this does not alter the emission angle, it does obscure the peaks at low electron beam energies, restricting the scope of the experiment.

## APPENDIX A

### NPS LINEAR ACCELERATOR

The linear accelerator at the Naval Postgraduate School is used to study radiation effects and damage, radiation characteristics and nuclear structure. The LINAC is capable of operating from approximately 15 MeV to 120 MeV. In this experiment, the usable range of energies was restricted to a range of about 60 MeV to 100 MeV. Figure A.1 below shows the general layout of the LINAC. The mylar foil stacks and the radiation detection equipment lie on the dashed line shown in the target area. Large magnets are used to deflect the incident electron beam away from the sensitive detector. Table A.1 provides a list of specifications for the LINAC (see for example [Refs. 5,6]).

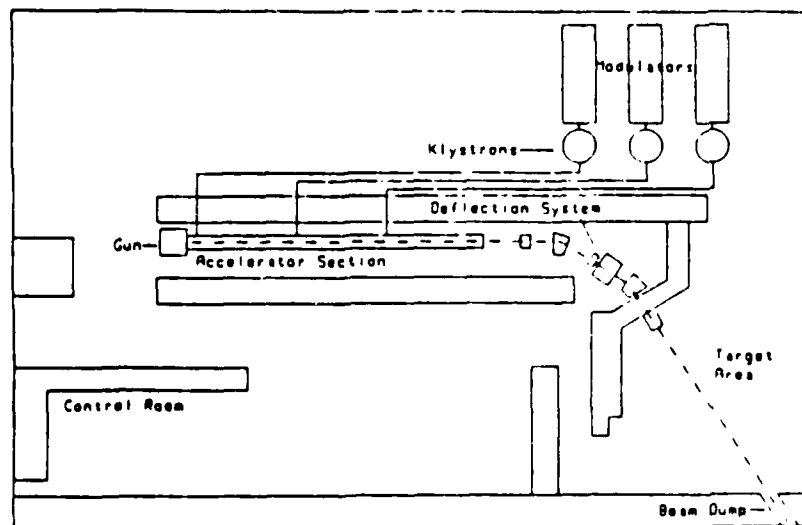


Figure A.1 NPS Linear Accelerator

TABLE A.1  
LINAC SPECIFICATIONS

Maximum energy	120 MeV
Overall length	~30 ft
Maximum average current	20 $\mu$ amps
Normal average current	3 $\mu$ amps
Number of Klystrons	3
Klystron peak power	21 MW
Klystron frequency	2.856 GHz
Pulse repetition frequency	60 Hz
Pulse duration	1.5 $\mu$ sec

## APPENDIX B

### HAMAMATSU LINEAR IMAGE SENSOR

A HAMAMATSU PCD Linear Image Sensor served as the x-ray detector for the experiment. The sensor is a self-scanning photodiode array designed specifically for multichannel spectroscopy [Ref. 11]. This was one of the first such uses of a HAMAMATSU array and generated much interest from the HAMAMATSU Corporation.

The array has 512 separate photodiodes. By reading each photodiode's output sequentially, a continuous scan of the transition radiation cone could be made. The output was then displayed on an oscilloscope or on a computer monitor (via appropriate software). Previous experiments similar to this at NPS used a gas proportional counter detector to measure the radiation cone. This required physically scanning the detector through the cone from top to bottom, a very time consuming process. The photodiode array gives instant measurements of the cone and allows immediate evaluation of adjustment needs.

The diodes are more sensitive to soft x-rays and the amount of sensitivity is dependent on the relative absorption at the particular energy (see Figure B.1). In addition to the reduced sensitivity, high energy radiation can damage the array. The dark current of the detector may

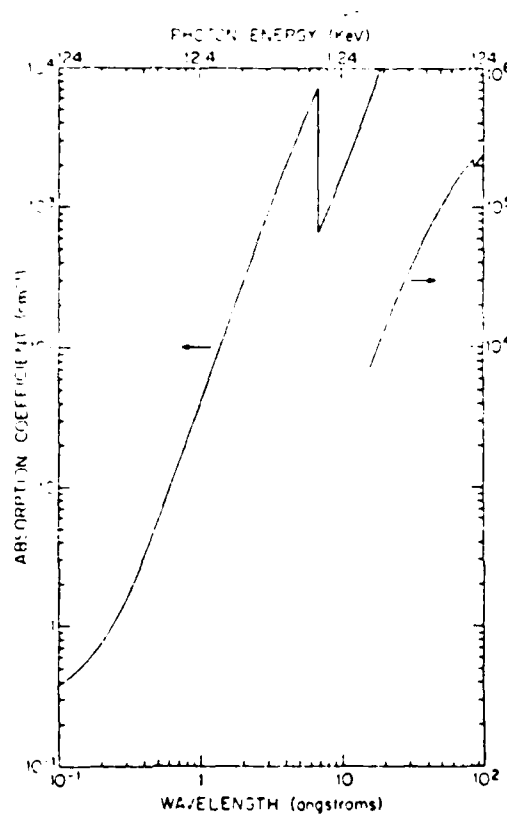


Figure B.1 X-ray Absorption Coefficient of Silicon as a Function of Wavelength and Photon Energy [Ref. 12:p. 3]

be permanently increased, especially in the regions where the incident radiation is highest. The radiation pattern can be "burned" into the detector, biasing all future measurements with the particular device.

Sensitivity is also affected by the temperature of the detector. Although information specific to the HAMAMATSU array was not available, similar arrays exhibit dark current



increases of a factor of about two for every 7°C increase in temperature [Ref. 12:p. 5].

## APPENDIX C

### TARGET STACK CONSTRUCTION

Construction of the coherent stack, the most complicated of the three stacks used, is discussed here. This stack was fabricated by Adelphi Technology, Inc. The stack was constructed using eight concentric steel rings. A mylar sheet was epoxy bonded to each ring at a temperature of 100°C. Due to the difference in thermal expansion coefficients of mylar and steel, the mylar foils were placed in tension when used at room temperature. The smallest steel ring was bolted to a flat steel plate. Remaining rings were attached in the same way in order of increasing size, except that a steel shim was added to the mating surfaces each time to provide the correct separation distance (see Figure C.1). Each stack had a nominal total foil thickness of 3.56  $\mu\text{m}$ . In the coherent stack, each mylar foil was separated by 8.5  $\mu\text{m}$ . The separation of foils in the incoherent stack was random.

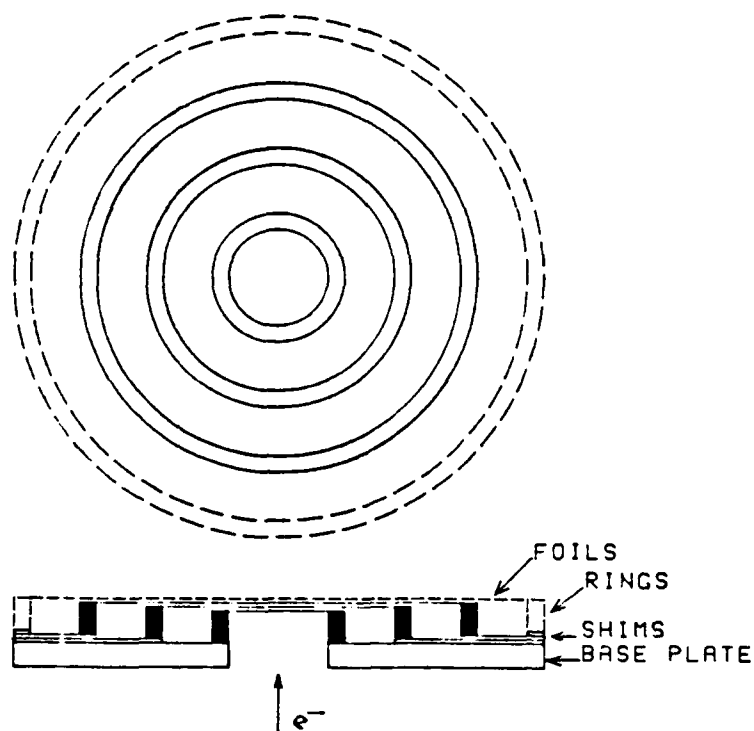


Figure C.1 Schematic Drawing of the Shimmed Concentric Ring Foil Stack. Shims are Used to Determine the Foil Spacing [Ref. 9:p. 22].

## APPENDIX D

### COMPUTER SIMULATION

The transition radiation simulation program solves for photon intensity per unit solid angle per unit frequency. The program is based on equation (3) using the development described in Chapter II. Variables in the program include:

- $\omega$  photon frequency;
- $\theta$  lower limit set at zero, upper limit inputted;
- $l_1, l_2$  interfoil spacing distance, foil thickness; varied by inputting various electron beam energies;
- $\omega_p$  plasma frequency.

The photon frequency was inputted in terms of energy. In order to obtain useful data to compare with experimental results, a range of energies was required. A range of energies from 0.1 keV to 4.0 keV in steps of 0.1 keV was specified. This range bracketed the soft x-ray range desired.

The actual radiation pattern includes contributions from various modes. To account for this, the program "sums" over a range of mode numbers. The range was determined using equation (10) in Chapter II:

$$\cos \theta_r = \frac{l_1 + l_2}{l_1 \sqrt{\epsilon_1} + l_2 \sqrt{\epsilon_2}} (1/\beta - r\lambda/(l_1 + l_2)) ,$$

where  $r$  is the mode number. One limit is set on the range of  $r$  by setting  $\theta_r = 0$  and solving for  $r$ ; the upper limit is set by inputting a maximum  $\theta_r$  and again solving for  $r$ . This limit is set (using experience with the program) to ensure the primary cone is within the range chosen.

The interfoil spacing and foil thickness were set equal to 8.5 microns and 3.5 microns, respectively. These values equal the actual values of the parameters on the coherent stack.

Electron beam energies were varied from 50 MeV to 120 MeV.

The plasma frequency was set in terms of energy and assumed to be equal to 24.1 eV. This value was determined from the equation

$$\omega_p = 3.72 \cdot 10^{-11} ((A \cdot N_0 \cdot \rho) / Z)^{1/2} ,$$

where  $A$  is the atomic number of the material,  $N_0$  is Avagadro's number,  $\rho$  is the density, and  $Z$  is the atomic weight. The program assumed all values for mylar were equal to the values for elemental carbon.

### LIST OF REFERENCES

1. Frank, I.M. and V.L. Ginzburg, "Radiation of a Uniform Moving Electron Due to Its Transition from One Medium into Another," Journal of Physics, Vol. 9, May 1945.
2. Cherry, M.L., G. Hartman, D. Muller and T.A. Prince, "Transition Radiation from Relativistic Electrons in Periodic Radiators," Physical Review, D. Vol. 10, December 1974.
3. Piestrup, M.A., P.F. Finman, A.N. Chu, T.W. Barbee, Jr., R.H. Pantell, R.A. Gearhart, and F.R. Buskirk, "Transition Radiation as an X-Ray Source," IEEE Journal of Quantum Electronics, Vol. QE-19, No. 12, December 1983.
4. Moran, M.J., B.A. Dahling and P.J. Ebert, "Measurement of Coherent Transition X-Rays," Physical Review Letters, Vol. 57, No. 10, p. 1223, 8 September 1986.
5. Yoon, S.K., Frequency Spectrum of Soft X-Ray Emission from Transition Radiation, Master's Thesis, Naval Postgraduate School, Monterey, California, December 1986.
6. Yim, C.H., Angular Distribution of Transition Radiation in the Soft X-Ray Spectrum, Master's Thesis, Naval Postgraduate School, Monterey, California, December 1986.
7. Fabjan, C.W. and W. Struczinski, "Coherent Emission of Transition Radiation," Physics Letters, 57B, p. 483, 1975.
8. Ter-Mikaelian, M.L., High Energy Electromagnetic Process in Condensed Media, New York, Wiley-Interscience, 1972.
9. Piestrup, M.A. and D.G. Boyers, "Detection of Coherent Transition Radiation and Its Application to Beam Diagnostics and Particle Identification," a Small Business Innovation Research proposal, 13 March 1987. (Private communication.)
10. "Transition Radiation Simulation (computer program)," Adelphi Technology, Inc., 1987. (Private communication.)

11. "PCD Linear Image Sensors (S3201 Series)," HAMAMATSU Technical Data Sheet, July 1985.
12. "Application of Reticon Photodiode Arrays as Electron and X-Ray Detectors," EG&G Reticon Application Notes No. 101, 1975.
13. Chu, A.N., M.A. Piestrup and R.H. Pantell, "Soft X-Ray Production from Transition Radiation Using Thin Foils," Journal of Applied Physics, Vol. 52, January 1981.
14. Chu, A.N., M.A. Piestrup, T.W. Barbee, Jr., and R.H. Pantell, "Transition Radiation as a Source of X-Rays," Journal of Applied Physics, Vol. 51, March 1980.

INITIAL DISTRIBUTION LIST

	No. Copies
1. Defense Technical Information Center Cameron Station Alexandria, Virginia 22304-6145	2
2. Library, Code 0142 Naval Postgraduate School Monterey, California 93943-5002	2
3. Professor John R. Neighbours, Code 61Nb Department of Physics Naval Postgraduate School Monterey, California 93943-5004	5
4. Professor Xavier K. Maruyama, Code 61Mp Department of Physics Naval Postgraduate School Monterey, California 93943-5004	5
5. Dr. M.A. Piestrup Adelphi Technology, Inc. 532 Emerson St. Palo Alto, California 94301	2
6. Lt. R.M. Robinson 2405 Garden Lane Lawton, Oklahoma 75301	3
7. Don Snyder, Code 61Ds Department of Physics Naval Postgraduate School Monterey, California 93943-5000	1



END

FEB.

1988

DTic